

# Electrothermal Performance of Heaters Based on Laser-Induced Graphene on Aramid Fabric

Iman Naseri, Morteza Ziaee, Zach N. Nilsson, Danielle R. Lustig, and Mostafa Yourdkhani\*

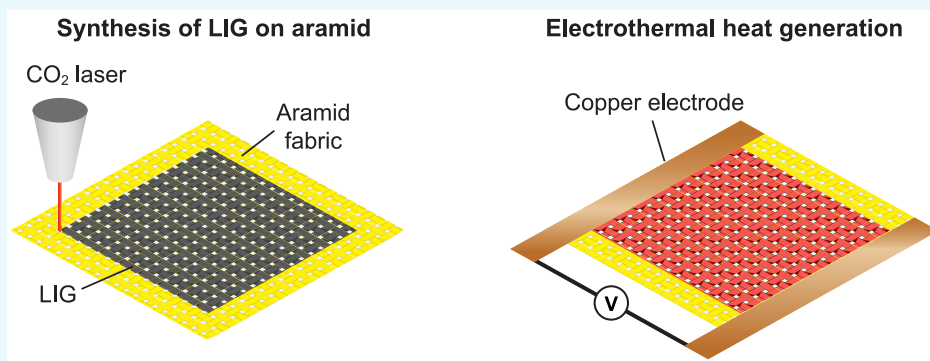
Cite This: *ACS Omega* 2022, 7, 3746–3757

Read Online

ACCESS |

Metrics &amp; More

Article Recommendations



**ABSTRACT:** Nanostructured heaters based on laser-induced graphene (LIG) are promising for heat generation and temperature control in a variety of applications due to their high efficiency as well as a fast, facile, and highly scalable fabrication process. While recent studies have shown that LIG can be written on a wide range of precursors, the reports on LIG-based heaters are mainly limited to polyimide film substrates. Here, we develop and characterize nanostructured heaters by direct writing of laser-induced graphene on nonuniform and structurally porous aramid woven fabric. The synthesis and writing of graphene on aramid fabric is conducted using a  $10.6\ \mu\text{m}$   $\text{CO}_2$  laser. The quality of laser-induced graphene and electrical properties of the heater fabric is tuned by controlling the lasing process parameters. Produced heaters exhibit good electrothermal efficiency with steady-state temperatures up to  $170\ ^\circ\text{C}$  when subjected to an input power density of  $1.5\ \text{W cm}^{-2}$ . In addition, the permeable texture of LIG–aramid fabric heaters allows for easy impregnation with thermosetting resins. We demonstrate the encapsulation of fabric heaters with two different types of thermosetting resins to develop both flexible and stiff composites. A flexible heater is produced by the impregnation of LIG–aramid fabric by silicone rubber. While the flexible composite heater exhibits inferior electrothermal performance compared to neat LIG–aramid fabric, it shows consistent electrothermal performance under various electrical and mechanical loading conditions. A multifunctional fiber-reinforced composite panel with integrated de-icing functionality is also manufactured using one ply of LIG–aramid fabric heater as part of the composite layout. The results of de-icing experiments show excellent de-icing capability, where a 5 mm thick piece of ice is completely melted away within 2 min using an input power of  $12.8\ \text{W}$ .

## 1. INTRODUCTION

Resistive heating has been widely used as a heat generation solution in a wide variety of applications, such as de-icing of aircraft structures, composite curing, water heating, and electric home appliances, due to the high heat generation efficiency and simplicity of use.<sup>1–4</sup> Metal alloys (e.g., Kanthal and Nichrome) have been traditionally used as resistive elements due to their low electrical resistance and high thermomechanical stability. However, such electrothermal materials suffer from high density and rigidity, making their use in emerging technologies (e.g., flexible heaters, wearable and portable devices) impractical.<sup>5,6</sup> The growing demand for Joule heating materials with unique properties, such as superior electrothermal performance, high degree of deformability, and low density, motivates the development of new materials and

processes.<sup>7</sup> For example, in the composite industry, the use of flexible heaters can allow for energy-efficient, out-of-oven manufacturing or in-the-field repair of composite parts with complex geometries.

Conductive nanomaterials are promising alternatives for fabricating highly deformable and efficient resistive heaters.<sup>8</sup> Fabrication of a resistive heater based on nanomaterials

Received: November 21, 2021

Accepted: January 11, 2022

Published: January 20, 2022



requires forming a continuous network of conductive nanoparticles to enable the flow of electrons and generating heat based on the electrothermal effect. A wide range of nanomaterials, such as silver nanowires,<sup>9</sup> copper nanowires,<sup>10</sup> graphene,<sup>11</sup> carbon nanotubes,<sup>12</sup> and MXene,<sup>13</sup> have been previously used for creating resistive heaters by generating conductive paths for the flow of electrons in various material systems. While nanomaterial-based resistive heaters offer great potential for fabricating highly efficient and multifunctional heaters, their widespread adoption on a commercial scale faces two major challenges. Production of such heaters typically involves multiple processing steps, including deposition and drying, which are undesirable from an economic point of view. In addition, scalability and large-scale utilization of such heaters are rather challenging and costly, making their use mainly limited to laboratory-scale research or specific applications.<sup>14</sup>

Laser-induced graphene (LIG) is a three-dimensional (3D) porous form of graphene that is synthesized by a rapid, facile, and scalable process and that exhibits excellent electrical and thermal conductivity, large surface area, mechanical robustness, and thermochemical stability.<sup>15–17</sup> The synthesis process of LIG involves lasing an appropriate precursor material with a CO<sub>2</sub>, UV, or visible-light laser source. Upon irradiation of the precursor material with a laser beam, the surface temperature locally increases via photothermal or photochemical effect, leading to direct conversion of the surface polymer layer into porous 3D graphene structures.<sup>18</sup> Several precursors, including polyimide, polyether sulfone, phenolic, and even wood, have been successfully converted into LIG in a single-step process.<sup>19</sup> Unlike conventional approaches for the synthesis of graphene and other nanomaterials, LIG synthesis process is highly scalable and inexpensive, is performed rapidly at ambient conditions, and allows for direct and concurrent patterning without any sophisticated masking or processing methods.<sup>20</sup> As a result, LIG has been used as an alternative to conventional conductive nanomaterials in a variety of applications such as sensing,<sup>21</sup> Joule heating,<sup>22</sup> water treatment,<sup>23</sup> actuators,<sup>24</sup> and energy storage devices.<sup>25</sup>

Resistive heaters based on LIG have been previously developed by directly writing graphene on polyimide films, where steady-state temperatures of more than 200 °C have been obtained under an input power of 1.4 W.<sup>26</sup> Such flexible heaters exhibit consistent performance after 10,000 bending cycles and are stable in high temperatures up to 225 °C. Additionally, the heaters offer better uniformity of temperature distribution compared to commercial counterparts while being less expensive. Large resistive heaters (20 × 20 cm<sup>2</sup>) based on LIG have also been fabricated using porous polyimide sheets as precursor materials instead of polyimide films.<sup>27</sup> The tailorable synthesis process of LIG has been exploited for creating heaters with multiple heating zones in one single step by changing the processing parameters during the lasing process.<sup>27</sup> Produced heaters were then used as an external heater for the out-of-oven curing of fiber-reinforced polymer composites, where an ~85% reduction in manufacturing energy was obtained compared to the conventional oven curing approach. In another work, composites with an integrated de-icing system based on LIG heaters were fabricated by combining extrusion-printing of polyamic acid solution on a cured composite laminate, followed by high-temperature imidization and laser-induced graphene synthesis process.<sup>28</sup> Although the creation of LIG patterns on

composites involved multiple processing steps, the resulting composites showed a good de-icing performance.

Development of LIG-based resistive heaters has been mainly limited to solid films of polyimide as the substrate material due to the ease of processing. Use of solid substrates, however, often results in shape distortion,<sup>27</sup> especially as the size of the lased region increases, and prevents easy encapsulation with other polymer resins or solutions in applications where integrated or sandwiched heaters are required. Porous substrates with the discontinuous distribution of polymer precursors, such as polymer fabrics or veils, allow for the easy infusion of polymer resins or solutions and minimize the shape distortion but provide a nonuniform, textured surface for LIG synthesis. This report describes the development of resistive heaters based on LIG–aramid woven fabrics as an alternative to polyimide film precursors. Aramid fabrics are less expensive substrate materials compared to polyimide films, provide a porous architecture for the easy infusion of solutions and resins, and are commonly used as fiber reinforcements in polymer composites. As a result, the LIG–aramid fabric heaters developed in the present study are compatible with most composite processing techniques and can readily be used to impart multifunctional properties to composite materials and structures.

Resistive heating of LIG-modified fabrics requires creation of a uniform and continuous network of LIG on the textured and nonuniform fabric architecture for the even distribution of electric current and heat generation throughout the fabric. In comparison with solid polymer films, the spacing between individual fibers within a tow or interyarn spacing can affect the continuity of the LIG network and spatial uniformity of heat generation. While LIG-modified aramid fabrics have been previously developed for protective clothing and composites with enhanced interlaminar mechanical properties and damage detection capability,<sup>29–31</sup> the use of LIG in those applications does not necessarily require integrity, continuity, and uniformity of the LIG layer within the entire plane of the fabric. To the best of our knowledge, resistive heating of LIG network synthesized on nonuniform, architected substrates (such as fabrics) has not been studied before.

The aim of the present work is therefore to investigate the electrothermal performance of resistive heaters based on LIG–aramid fabric and understand the role of various processing parameters on the quality and performance of resulting heaters. The effect of input laser power on the quality of LIG–aramid is studied by characterizing the morphology and chemical composition of the produced LIG. Detailed experiments are carried out to determine the relationship between lasing process parameters (i.e., input laser power, scan rate, and pulse per inch, PPI) and electrical properties as well as the Joule heating performance of LIG–aramid fabric heaters. Fabric heaters are then used to create flexible and stiff composites using two different types of polymer resins and to demonstrate the easy integration of fabric-based heaters in polymer matrices for developing multifunctional polymer composites. Highly flexible LIG heaters are prepared by the impregnation of LIG–aramid fabrics with a polydimethylsiloxane silicone rubber. While the addition of silicone rubber might adversely affect the electrothermal efficiency of heaters, it enhances their durability and reliability, which is ideal for use in applications where flexible and robust heaters are required. In addition, an aramid composite panel containing a top layer of LIG–aramid is fabricated and the de-icing performance of the resulting

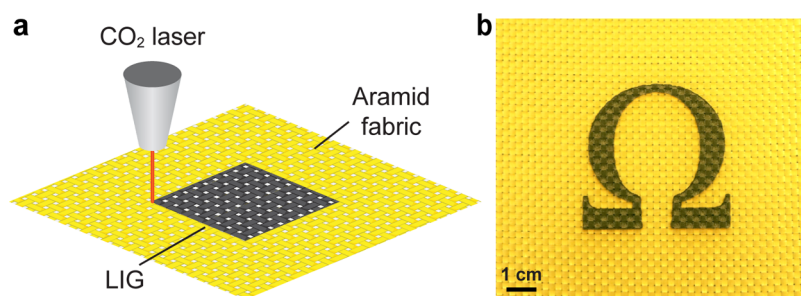


**Figure 1.** Writing laser-induced graphene (LIG) on aramid fabric. (a) Schematic representation of the lasing process. (b) Example of an LIG pattern created on aramid fabric.

multifunctional composite is demonstrated. Owing to the facile and scalable synthesis and writing of LIG along with the easy impregnation of the substrate aramid fabric with polymeric materials, the heaters developed in this study can be used in a wide variety of applications where flexible or integrated heaters are required.

## 2. EXPERIMENTAL SECTION

**2.1. Preparation of LIG–Aramid Fabrics and Composites.** Woven aramid (Kevlar) fabric (plain weave, thickness = 230  $\mu\text{m}$ , areal weight = 140 gsm, fiber linear mass density = 0.127  $\text{g m}^{-1}$ ) was purchased from ACP Composites and used as received. LIG was synthesized on aramid fabric using a 10.6  $\mu\text{m}$   $\text{CO}_2$  laser (ILS 12.15 platform, 75 W, Universal Laser Systems) in a raster mode. Various processing parameters including laser power, scan rate, and pulse per inch were used to tailor and study the quality and properties of the resulting LIG. For the preparation of flexible composite heaters, one layer of LIG-patterned fabric ( $25 \times 40 \text{ mm}^2$ ) was impregnated with a polydimethylsiloxane silicone rubber (SYLGARD 184, Dow Corning) by the drop-casting method and cured in an oven at 70  $^\circ\text{C}$  for 8 h. The resin used in the drop-casting technique was prepared by manually mixing 1 g of the hardener with 10 g of the silicone resin for 5 min. For the preparation of the composite panel with an integrated de-icing surface layer, eight plies of aramid fabric including one top layer of LIG–aramid were impregnated with a thermoset resin using the hand-layup technique, vacuum-bagged, and cured in an oven at 70  $^\circ\text{C}$  for 12 h. The resin system used for the manufacture of the composite panel was based on dicyclopentadiene (DCPD) and prepared according to the procedure developed by Robertson et al.<sup>32</sup> Briefly, dicyclopentadiene (Sigma-Aldrich, CAS Number: 77-73-6) was first mixed with 5-ethylidene-2-norbornene (Sigma-Aldrich, CAS Number: 16219-75-3) at a 95:5 weight ratio to depress its melting point. Then, 6 g of this resin solution was mixed with another solution consisting of 3.85 mg of second-generation Grubb's catalyst (Sigma-Aldrich, CAS Number: 246047-72-3) and 1.2  $\mu\text{L}$  of tributyl phosphite (TCI America, CAS Number: 102-85-2) dissolved in 500  $\mu\text{L}$  of phenylcyclohexane (Sigma-Aldrich, CAS Number: 827-52-1).

**2.2. Structural Characterization of LIG.** The morphology of pristine aramid fabric and LIG was imaged using a JEOL JSM-5800 field emission scanning electron microscope (FESEM) at an accelerating voltage of 1 kV. The as-produced LIG sample was imaged without any surface coating step due to the intrinsic electrical conductivity of the LIG layer, whereas the surface of the pristine aramid sample was sputter-coated with a 10 nm thick layer of gold. Raman spectra were collected

using a Horiba THz Raman system (26 mW, 532 nm) focused through a 10 $\times$  microscope objective (Olympus) mounted on an Olympus IX73 inverted microscope. A Horiba iHR550 spectrometer was used to disperse the Raman signal on a Horiba Synapse back-illuminated CCD camera for detection. Electrical measurements were conducted using a DM285 FLIR multimeter. X-ray photoelectron spectroscopy (XPS) was performed using a Physical Electronics 5800 series Multi-Technique ESCA system with a monochromatic Al  $K\alpha$  ( $h\nu = 1486.6 \text{ eV}$ ) source operated at 350.0 W. An electron flood gun was used for charge neutralization. High-resolution scans were collected with a pass energy of 23.5 eV and an interval of 0.1 eV/step. The instrument pressure was  $5 \times 10^{-8}$  torr or lower during data acquisition.

**2.3. Characterization of Electrothermal Performance.** Electrothermal performance of resistive heaters was evaluated using specimens with a  $15 \times 15 \text{ mm}^2$  effective heating area prepared under various processing conditions. A nickel-filled conductive paste (Pyro-Duct 598 A, Aremco) was used to attach copper electrodes to both ends of heaters. Various voltages were supplied to heaters using a direct current (DC) power supply (9206, B&K Precision). The temperature at the center of heaters was measured using a T-type thermocouple and recorded by a LabView program. A FLIR T540 infrared thermal camera was also used to measure the temperature distribution and stability of heaters under static and cyclic electrical loading conditions.

## 3. RESULTS AND DISCUSSION

**3.1. Synthesis of LIG on Aramid Fabric.** The manufacturing process of LIG–aramid fabric heaters is schematically shown in Figure 1a. Upon irradiation of aramid fabric with a  $\text{CO}_2$  laser beam, the material is converted into porous graphene via a photothermal process. Unlike conventional nanomaterial-based Joule heating methods, which require handling and deposition of nanomaterials in multiple processing steps, the synthesis and writing of graphene on aramid fabric is conducted in one simple step. In addition, highly customized and geometrically complex patterns of LIG can readily be written on aramid fabric without the need for using any masks (Figure 1b).

The microstructure, composition, and morphology of LIG–aramid were studied using Raman spectroscopy, X-ray photoelectron spectroscopy (XPS), and scanning electron microscopy (SEM), respectively. Raman spectra of aramid fabric before and after laser treatment are shown in Figure 2a. The characteristic peaks of aramid at 1509, 1566, 1606, and 1640  $\text{cm}^{-1}$  disappeared after laser scribing, and three new bands formed at 1337, 1565, and 2667  $\text{cm}^{-1}$ . These new bands

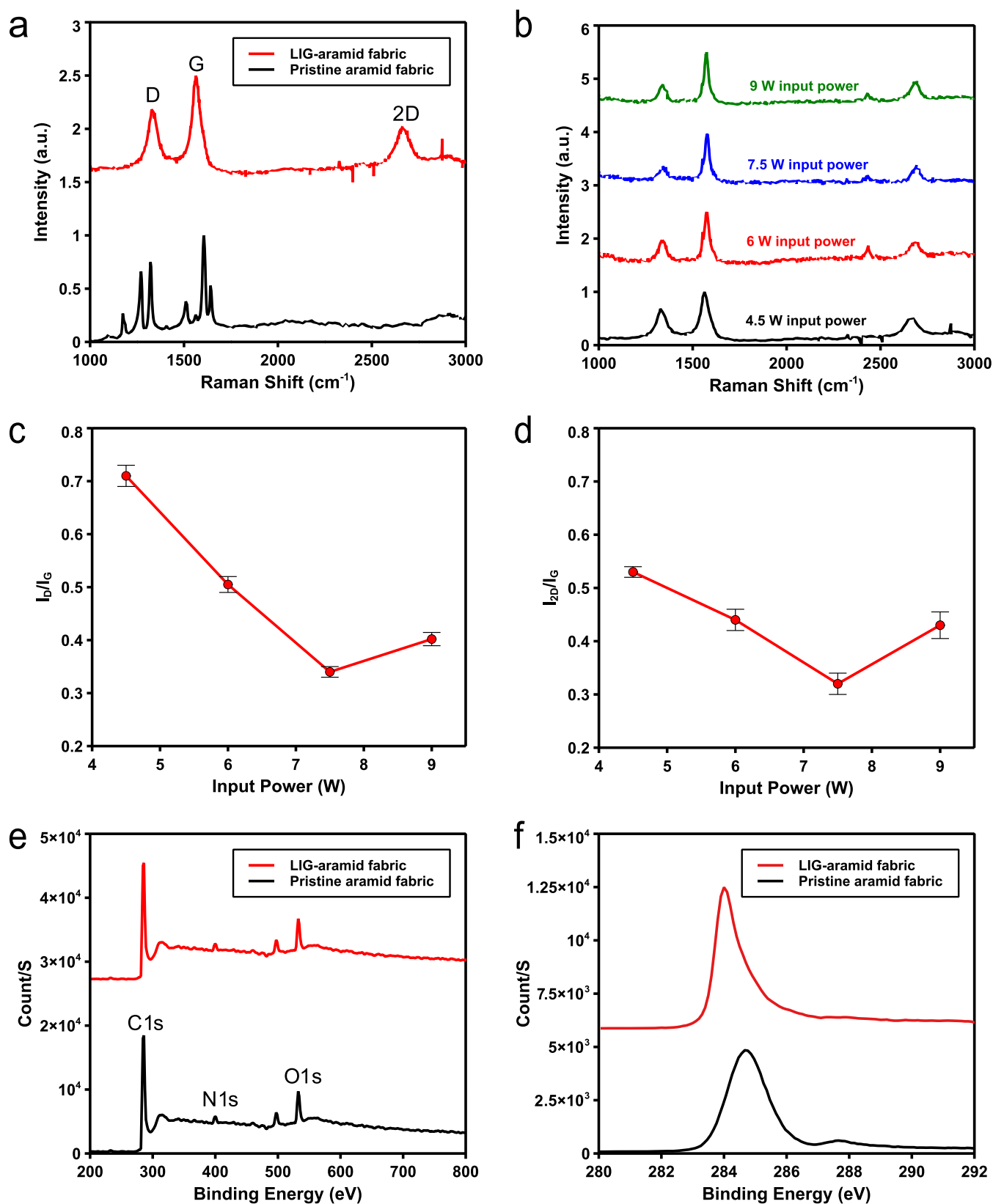


**Figure 2.** Characterization of the microstructure and composition of LIG-aramid. (a) Raman spectra of aramid fabric before and after laser treatment under an input laser power of 4.5 W, a PPI of 800, and a scan rate of  $90 \text{ mm s}^{-1}$ . (b) Effect of laser input power on the Raman spectra of LIG. (c, d) Variation of D/G and 2D/G peak intensity ratios as a function of input laser power, respectively. (e) XPS general survey before and after laser treatment (input laser power = 9 W, PPI = 800, and scan rate =  $90 \text{ mm s}^{-1}$ ). Upon the laser treatment, the ratio of N 1s to C 1s peak intensities in aramid decreases from 0.238 to 0.226 and the ratio of O 1s to C 1s peak intensities decreases from 0.433 to 0.391. (f) High-resolution XPS carbon (C 1s) spectra before and after laser ablation, indicating the removal of the peak around 288 eV and changing the symmetry of the main peak after the lasing treatment.

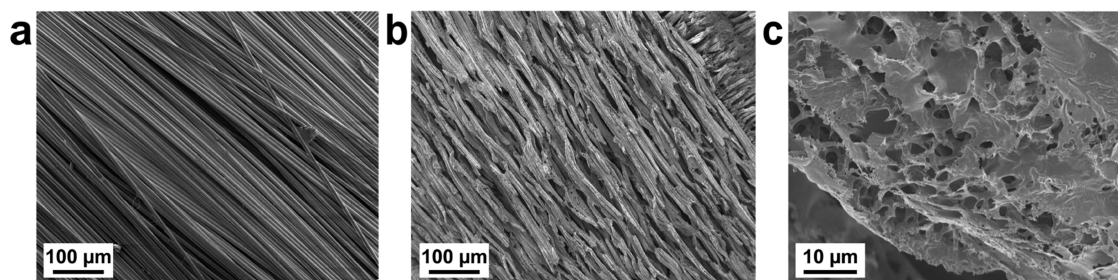


**Figure 3.** Morphological characterization of aramid fabric before and after laser treatment using SEM imaging (input power = 9 W, PPI = 800, and scan rate = 90 mm s<sup>-1</sup>). (a) Pristine aramid fabric. (b, c) LIG-aramid fabric at two magnifications.

are representative of the D-band, G-band, and 2D-band of the graphitic structure, respectively.<sup>33</sup> Specifically, the D-band is related to defects, bent sp<sup>2</sup> bonds, and vacancies, while the G-band is the first-order Raman band of all sp<sup>2</sup>-hybridized carbons. The relative intensities of these three peaks are a measure of the quality of graphene. The intensity ratio of D-band to G-band ( $I_D/I_G$ ) is a measure of the defect level in the graphitic structure, whereas the intensity ratio of 2D-band to G-band ( $I_{2D}/I_G$ ) is related to the number of graphene layers stacked in the *c*-axis. Raman spectrum of a high-quality graphene typically exhibits a low D/G-band ratio and high 2D/G-band ratio.<sup>34</sup> Although the quality of graphene produced on an aramid precursor is not as good as those synthesized on a polyimide precursor, as also previously reported for LIG-aramid,<sup>30</sup> the resulting LIG is still conductive enough to exhibit substantial Joule heating capability.

The effect of laser input power on the quality of the resulting LIG is shown in Figure 2b–d. An increase in the input laser power first decreases the defect levels but then results in increased defect quantity (Figure 2c). This observation can be attributed to the temperature increase during the lasing process, which is directly affected by the input laser power. When the input laser power is low, the graphitization temperature is not high enough for achieving a high degree of crystallinity in the graphitic structure, resulting in high defect levels. As the input laser power increases, the conversion of precursor into graphitic structures occurs at higher temperatures, leading to higher levels of order. However, thermal oxidation at high input power caused by excessively high temperatures results in the formation of high amounts of defects in the graphitic structure. In addition to the influence on the level of defect, the input laser power also affects the number of layers in the LIG. The values of  $I_{2D}/I_G$  ratios reveal that multilayer graphene is formed during the lasing process (Figure 2d).

The surface compositions of untreated and treated fabrics were characterized by XPS measurements (Figure 2e,f). The survey spectra of the neat aramid fabric show three peaks at 289, 400, and 550 eV, which are indicators of carbon, nitrogen, and oxygen elements, respectively (Figure 2e). A comparison of the survey spectra before and after laser scribing reveals a slight reduction in the atomic percentages of nitrogen and oxygen elements. This reduction in concentrations of oxygen and nitrogen elements is also confirmed by the high-resolution carbon spectra of LIG (Figure 2f). In addition, the asymmetric peak of the LIG-aramid fabric at low binding energies is another evidence for the formation of graphitic structures (Figure 2f).<sup>35</sup>

The morphological changes of aramid fabric after laser treatment were determined using SEM imaging. While

untreated aramid fibers exhibit a very smooth surface (Figure 3a), the treated fibers show a relatively rough and porous surface structure (Figure 3b,c). The higher-magnification micrograph in Figure 3c shows the sheet-like porous structure of the scribed fibers, caused by the release of gaseous products during the lasing process due to the photochemical breakage of chemical bonds, such as C–N and C=O.<sup>36</sup>

**3.2. Electrothermal Characterization of LIG-Aramid Fabric.** Developing efficient resistive heaters based on LIG-aramid requires a thorough understanding of the effect of processing parameters on the electrothermal performance of modified fabrics. Three key processing parameters, which can directly affect the quality and performance of heaters, are input laser power, laser scan rate, and pulse per inch (PPI). The effects of these three lasing process parameters on the electrical and electrothermal performance of LIG-aramid heaters are shown in Figure 4. As the laser power increases from 4.1 to 6.1 W, the electrical resistance of modified fabrics decreases from 422 to 42 Ω (Figure 4a). Further increase in the laser power results in a steady drop in the electrical resistance such that a resistance of 19 Ω is achieved at an input laser power of 8.9 W. Incomplete conversion of aramid precursor to graphene along with the relatively low quality of graphene is responsible for the relatively high electrical resistance of LIGs at low input laser powers. With an increase in the laser power, a thicker layer of aramid is converted into graphene and the defect level in the graphitic structure is decreased, leading to a lower measured resistance.

The electrothermal performance of nanostructured heaters produced by various input laser powers was determined by applying a constant voltage of 10 V across specimens and measuring their time-dependent temperature profiles (Figure 4b). As the driving voltage is applied, the temperature of resistive heaters rapidly increases until a steady-state temperature is reached. Additionally, higher steady-state temperatures are observed for heaters produced by higher input laser powers, indicating the significance of graphene quality and electrical conductivity on the electrothermal performance of LIG-based heaters. This improvement in electrothermal performance can be explained by the inverse relationship between the generated heat (*Q*) and heater resistance (*R*) for a given input voltage<sup>37</sup>

$$Q = \frac{V^2}{R} \quad (1)$$

As the resistance of heaters decreases, more electric current can pass through the heater when subjected to a constant input voltage, leading to a higher frequency of collision between

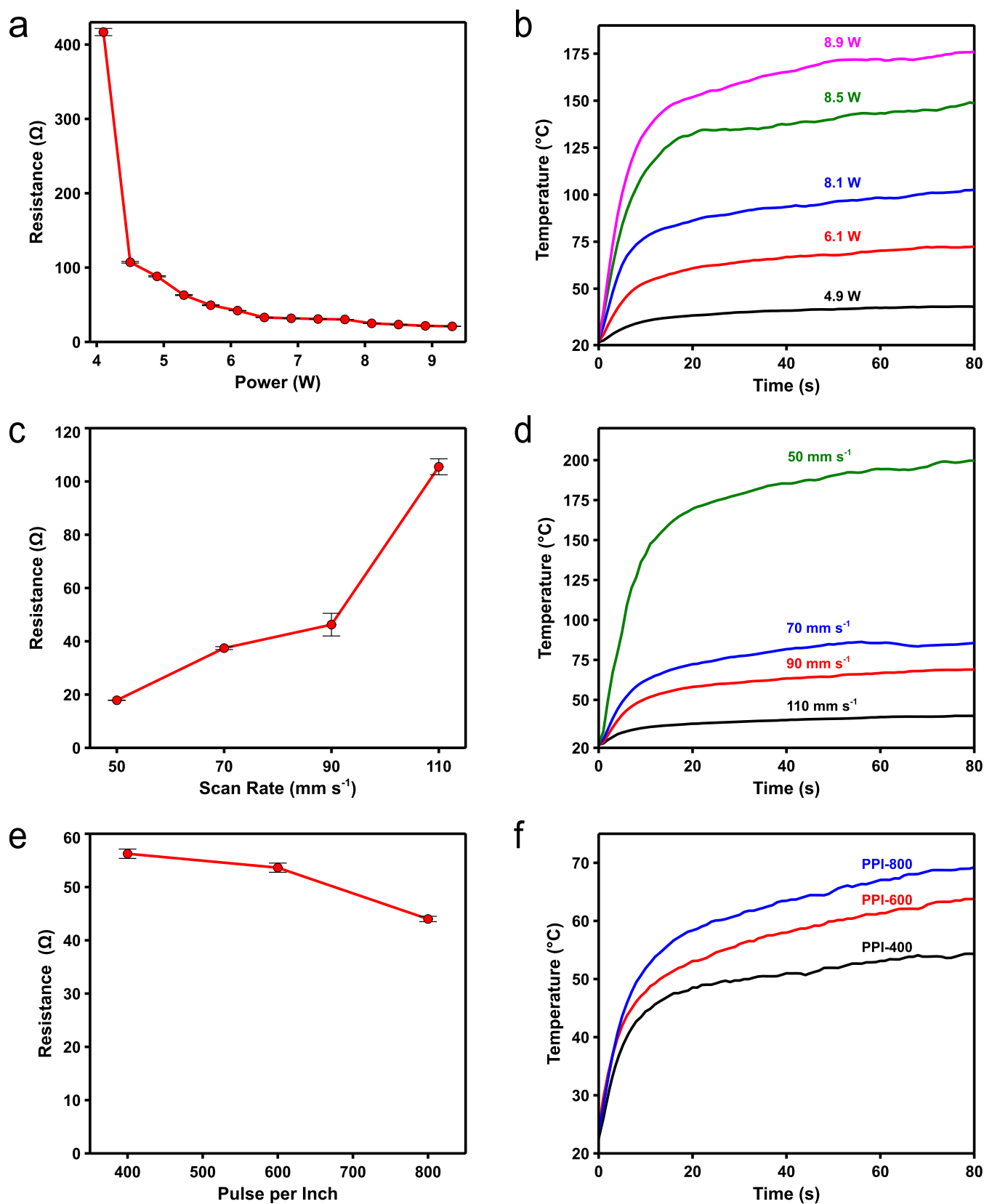


**Figure 4.** Effect of laser processing parameters on electrical properties and time-dependent electrothermal performance of LIG-aramid fabrics. (a, b) Electrical resistance and electrothermal response of LIG samples prepared by various input laser powers at a fixed scan rate of  $90 \text{ mm s}^{-1}$  and a PPI of 800, respectively. (c, d) Electrical resistance and electrothermal response of LIG samples prepared by various scan rates at a fixed input laser power of 6.1 W and a PPI of 800, respectively. (e, f) Electrical resistance and electrothermal response of LIG samples prepared by various PPI values at a fixed laser input power of 6.1 W and a scan rate of  $90 \text{ mm s}^{-1}$ .

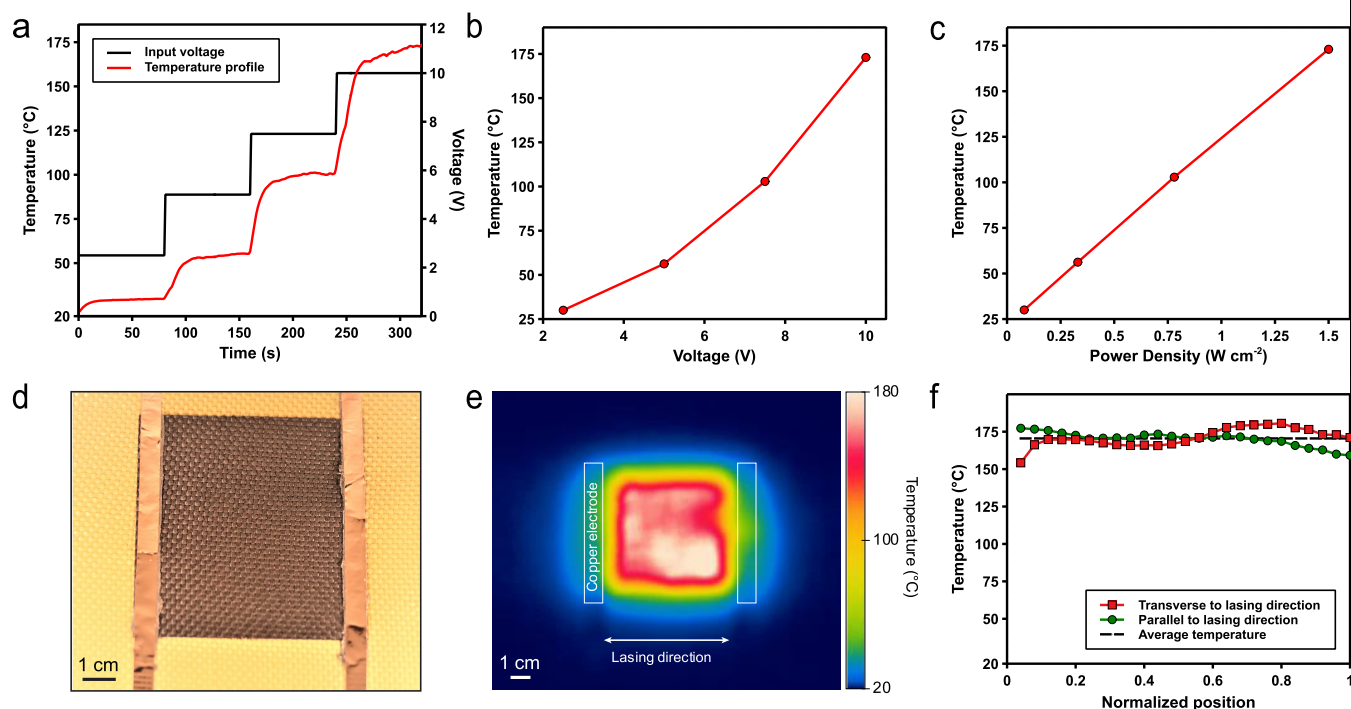


**Figure 5.** Electrothermal performance of LIG–aramid fabric heaters under various input voltages. (a) Temperature profile of an LIG–aramid heater (input power = 8.9 W, PPI = 800, and scan rate = 90 mm s<sup>-1</sup>) in response to an increasing input voltage load. (b) Steady-state temperature of the heater in panel (a) as a function of input voltage. (c) Relationship between the steady-state temperature of the heater in panel (a) and power density. (d, e) Digital and thermal infrared images of a large LIG–aramid heater (effective heating area = 35 cm<sup>2</sup>), respectively. (f) Temperature distribution along the midlines of the sample shown in panels (d, e). The midline directions are parallel and transverse to the lasing direction.

electrons and increased heat generation as a result of energy loss.

Scan rate is another processing parameter that is used to control the speed of laser beam movement across the specimen. A series of heaters were prepared under a fixed input power of 6.1 W, a PPI of 800, and various scan rates to understand the effect of scan rate on the performance of heaters (Figure 4c,d). As shown in Figure 4c, heater resistance increases with an increase in the scan rate, where a low electrical resistance of 16 Ω is measured for a scan rate of 50 mm s<sup>-1</sup>. The electrothermal performance of heaters improves at lower lasing speeds, where steady-state temperatures of up to 200 °C can be obtained using a lasing speed of 50 mm s<sup>-1</sup> (Figure 4d). According to these results, heaters produced at low input powers and low scan rates exhibit similar performance to those produced at high input powers and high scan rates although the latter processing condition is more desirable from the productivity point of view.

The effect of PPI on the quality and performance of LIG–aramid fabric heaters is shown in Figure 4e,f. PPI is a processing parameter that is used to control the number of laser pulses per linear inch of engraving. Fabric heaters were prepared under various PPIs while fixing the input power to 6.1 W and the scan rate to 90 mm s<sup>-1</sup>. The electrical resistance of LIG–aramid decreases from 56 to 42 Ω as PPI varies from 400 to 800 (Figure 4e). Considering the nonuniform, textured architecture of the aramid fabric, an increase in the PPI allows for lasing a higher number of points along the lasing direction and improving the continuity and uniformity of the produced

graphene network on the uneven substrate. This observation, however, is in contrast to the results of LIG synthesis on uniform polyimide films, where an increase in PPI results in reduced energy density delivered by each pulse, leading to an increase in the average resistance of the LIG.<sup>38</sup> The reduction in electrical resistance observed in Figure 4e is associated with a 15 °C increase in the steady-state temperature of heaters during the electrothermal tests under an input voltage of 10 V (Figure 4f).

We performed additional experiments to understand the electrothermal response of heaters to various applied voltages. For these experiments, the temperature profile of a heater produced under an input laser power of 8.9 W, a PPI of 800, and a scan rate of 90 mm s<sup>-1</sup> was determined by varying the value of voltage applied across the heater (Figure 5a). The steady-state temperature of the heater increased quadratically as a function of the applied voltage (Figure 5b), verifying that the response of the resistive heater follows Joule's law. The consumed power density for reaching a temperature of 170 °C from room temperature is 1.5 W cm<sup>-2</sup> (Figure 5c), which is equivalent to a heating performance of 100 °C cm<sup>2</sup> W<sup>-1</sup>. While this heating performance is slightly lower than that of LIG heaters produced using PI films as a precursor (131 °C cm<sup>2</sup> W<sup>-1</sup>),<sup>26</sup> it is sufficiently high to meet the heating requirements of a wide range of applications.

A larger heater (effective heating area = 35 cm<sup>2</sup>) was also produced under the same processing condition (i.e., input power = 8.9 W, scan rate = 90 mm s<sup>-1</sup>, and PPI = 800) to demonstrate the scalability of the manufacturing process and

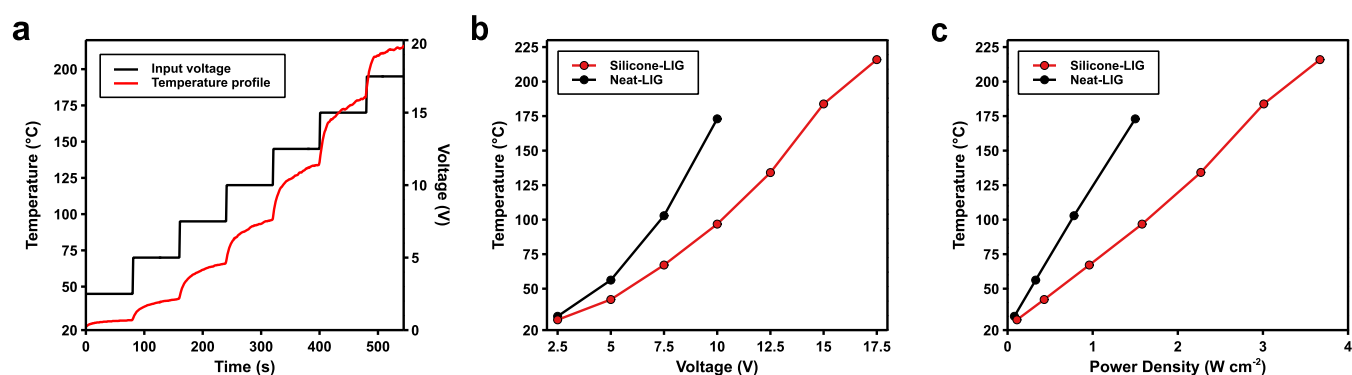


**Figure 6.** Electrothermal response of a flexible silicone-encapsulated LIG–aramid fabric. (a) Temperature profile of the encapsulated heater in response to an increasing input voltage load. (b, c) Steady-state temperature of both encapsulated and unencapsulated heaters as a function of applied voltage and power density, respectively.

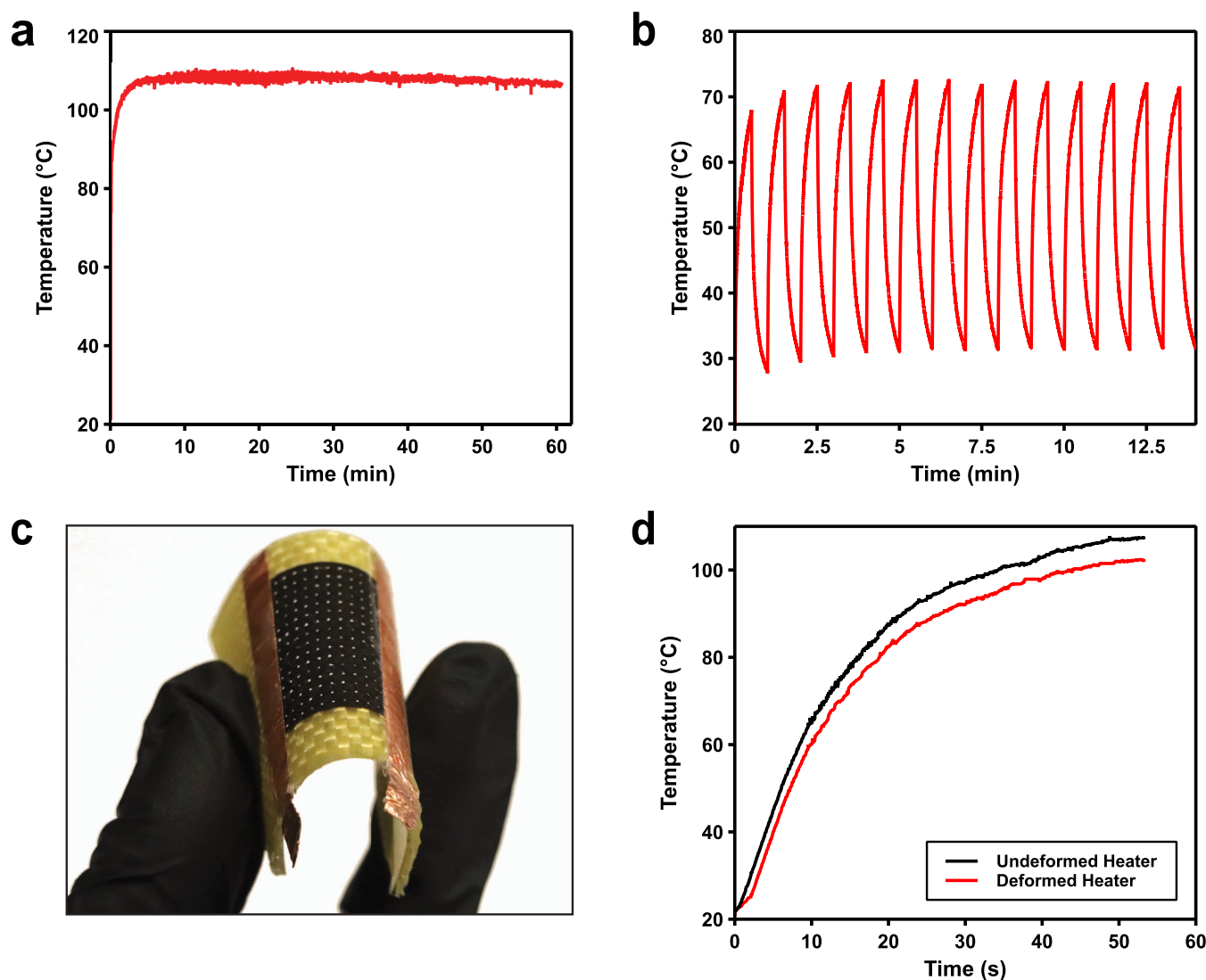


**Figure 7.** Electrothermal performance of the silicone-encapsulated LIG–aramid fabric under various electrical and mechanical loading conditions. (a) Long-term stability test at a constant input voltage of 10 V. (b) Cyclic stability test by varying the applied voltage between 0 and 10 V within 30 s time intervals. (c) Digital image of the bent encapsulated LIG–aramid fabric. (d) Time-dependent temperature profile of the heater in bent (radius of curvature of  $\sim 7$  mm) and flat configurations.

resistive heating performance of produced heaters (Figure 5d). The thermal infrared image of the heater shows an even distribution of temperature (average temperature = 170 °C)

with a 10 °C variation throughout the heater in response to a power density of 1.3 W cm<sup>-2</sup> (Figure 5e). In addition, similar temperature profiles were measured along the two midlines of

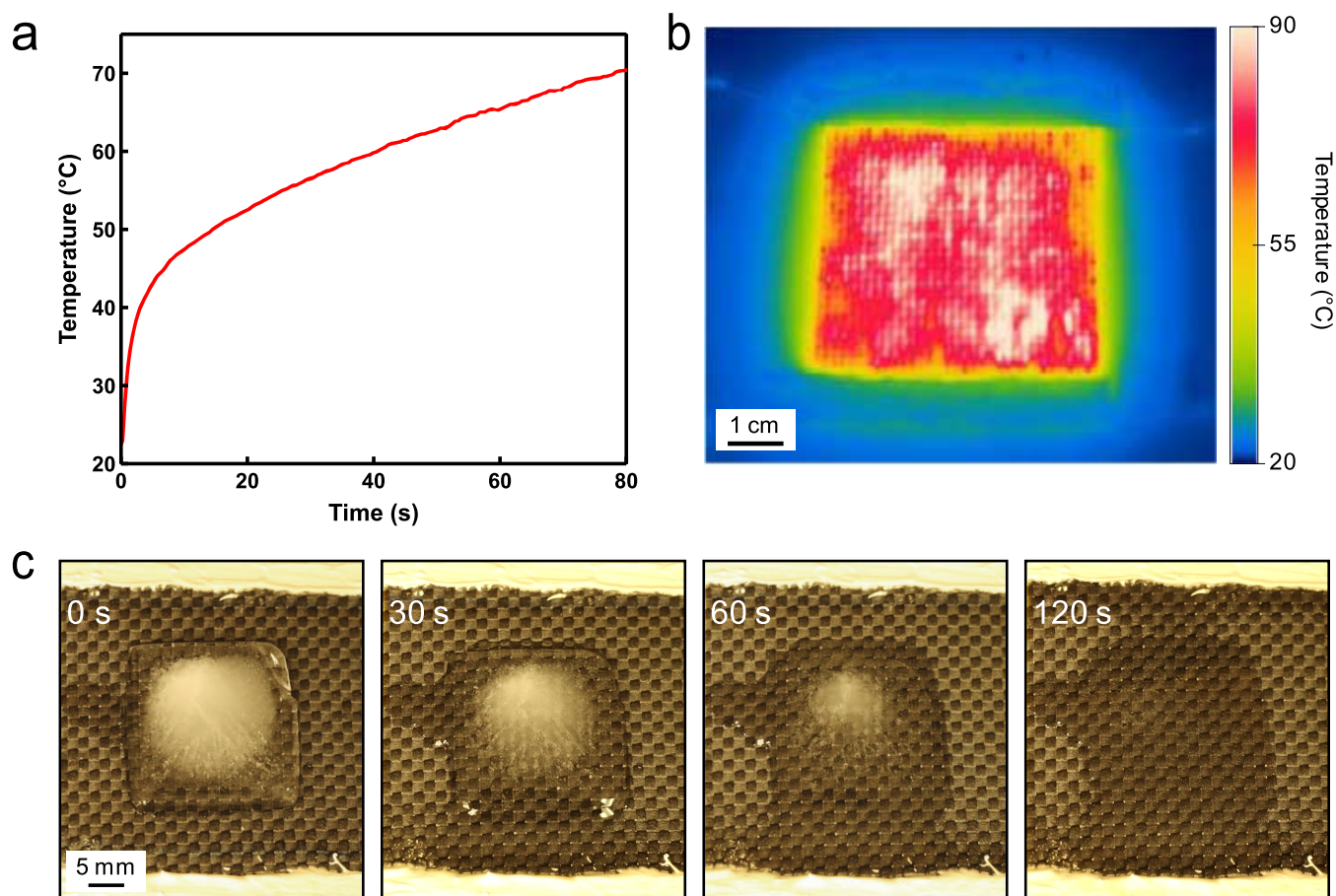


**Figure 8.** Manufacturing a multifunctional aramid-thermoset composite laminate with an integrated ply of LIG–aramid fabric. (a) The average temperature profile of the cured composite when subjected to an input voltage of 15 V. (b) Thermal infrared image of the composite laminate at  $t = 80$  s. (c) Demonstration of the de-icing functionality of the resulting composite laminate. A  $20 \times 20 \times 5$  mm<sup>3</sup> piece of ice is completely melted away within 2 min after applying an input voltage of 15 V across the laminate.

the sample (Figure 5f); however, a more uniform temperature distribution was observed along the lasing direction compared to that along the transverse direction. This directional difference in temperature distribution is attributed to the more controlled and uniform creation of graphene along the lasing direction compared to that along the transverse direction.

**3.3. Silicone-Encapsulated LIG–Aramid Fabric.** While LIG-modified films and fabrics exhibit excellent electrothermal performance, they are prone to mechanical damage during handling and service due to the brittle structure of LIG layers.<sup>26</sup> Loss of the conductive LIG layers can consequently result in increased resistance and degradation of the performance of LIG heaters. We improve the mechanical robustness of LIG–aramid fabrics by encapsulating them with silicone rubber and protecting the LIG structure against mechanical damages and scratches. Although silicone rubber is an intrinsically insulating polymer, we observed no significant change in the electrical resistance of LIG after encapsulation with silicone. We hypothesize that the resistance of LIG does not vary when encapsulated by silicone due to two competing effects. The presence of the electrically insulating rubber is typically expected to increase the overall resistance of the LIG structure after filling the porous spacing within graphene layers. However, deformation of the LIG structure due to cure shrinkage of silicone can lead to compaction of the LIG network and therefore a reduction in resistance. As a result, no

significant change in the resistance of LIG-modified fabric was observed upon the encapsulation process. However, the electrothermal performance of the LIG fabric remarkably decreased upon encapsulation by silicone rubber (Figure 6a). For example, the steady-state temperature of the composite heater is  $\sim 100$  °C under an applied voltage of 10 V, whereas the equilibrium temperature of the unencapsulated fabric heater is  $\sim 170$  °C under the same condition (Figure 6b). The difference in the equilibrium temperature ( $T_{\text{eq}}$ ) of encapsulated and unencapsulated heaters can be explained by the following equation<sup>39</sup>

$$T_{\text{eq}} = \frac{\frac{V^2}{R} - Q_{\text{loss}}}{mC_p} + T_0 \quad (2)$$

where the first term represents the amount of heat generated by the Joule heating effect,  $m$  is the mass of the heater,  $C_p$  is the heat capacity of the heater,  $Q_{\text{loss}}$  is the amount of heat dissipated via any mechanisms, and  $T_0$  is the ambient temperature. Since the resistance of the heater remains unchanged after adding silicone rubber, the amount of heat generated via the Joule heating effect remains constant. However, the thermal mass of the heater increases when adding silicone encapsulant, resulting in a reduced equilibrium temperature of the composite heater. In addition, the presence of silicone rubber can facilitate heat dissipation to substrate via

conduction heat transfer. As a result, the higher thermal mass of the composite heater and the increased heat loss to the surrounding are responsible for the observed inferior performance of the composite heater compared with those of as-prepared LIG–aramid fabric heaters. Similarly, the composite heater requires higher input electric power for reaching a given steady-state temperature compared to the LIG–aramid fabric without silicone rubber (Figure 6c).

The electrothermal stability of composite heaters was determined using both electrical static and cyclic loads to evaluate the time-dependent and dynamic response of heaters to applied power (Figure 7). For static electrothermal tests, a constant voltage of 10 V was applied on the heater while monitoring its average temperature over time (Figure 7a). In dynamic electrothermal tests, the applied voltage was intermittently varied between 0 and 10 V during 30 s time intervals (Figure 7b). The steady-state temperature of the composite resistive heater did not significantly change even after 1 h of continuously applying electric power. Similarly, the results of the cyclic electrothermal stability test reveal that the performance of the heater is consistent under electrical cyclic loading conditions, further verifying the reliability and reproducibility of produced composite heaters. In addition, the encapsulated LIG heater could preserve its heat generation capability when deformed from the original flat shape to a bent geometry (Figure 7c,d). However, a small difference ( $\sim 5$  °C) between steady-state temperatures of deformed and undeformed heaters was observed, which is due to a slight increase in the resistance of the heater under bending deformation.

**3.4. Aramid Composite Laminate with Integrated De-icing Functionality.** The fabric structure of the aramid precursor used for the synthesis of LIG in this study is ideal for the easy integration of LIG-based heaters into fiber-reinforced polymer composites and imparting multifunctional properties such as de-icing to the composite materials. The integrated fabric heater can eliminate the need for parasitic heavy metallic resistive heaters traditionally used for de-icing of composite structures while contributing to the mechanical reinforcement of the host composite. We manufactured an aramid composite laminate with a thermoset matrix to demonstrate the de-icing capability of composites with an integrated fabric heater. Composite layup was prepared by placing one ply of LIG–aramid fabric on top of seven pristine aramid fabric plies. The electrothermal response of the fiber-reinforced composite laminate is shown in Figure 8a,b. The average temperature of the laminate quickly increases to  $\sim 70$  °C within 80 s in response to an applied voltage of 15 V, which is high enough to quickly melt the surface ice layers. The de-icing capability of the composite laminate is further demonstrated by placing a  $20 \times 20 \times 5$  mm<sup>3</sup> piece of ice on the laminate and applying the same voltage (i.e., 15 V) across the laminate. As shown in Figure 8c, the ice layer completely melts away within 2 min after applying the input voltage, indicating the excellent de-icing performance of the manufactured composite laminate with an integrated LIG–aramid fabric.

## 4. CONCLUSIONS

We have demonstrated that a textured, woven aramid fabric can be successfully used as an inexpensive precursor for fabricating LIG-based resistive heaters with a high electrothermal efficiency. The quality and performance of fabric heaters were directly affected by the key processing parameters, namely, input laser power, scan rate, and pulse per inch of

engraving. The electrothermal response of produced LIG heaters followed Joule's law, where a linear correlation was obtained between the steady-state temperature of heaters and the square of the input voltage. The fabric structure of LIG heaters allowed for facile impregnation with polymer resins for the development of integrated heaters and multifunctional composites. Two types of thermosetting resins were used to fabricate flexible and stiff composites using LIG–aramid fabric for various applications. Highly flexible and stable heaters were prepared by the impregnation of LIG-modified aramid fabric with silicone rubber, while a multifunctional fiber-reinforced composite laminate with de-icing functionality was manufactured using dicyclopentadiene resin system. The LIG–aramid fabric heaters developed in this study can be used in a wide variety of applications including out-of-oven curing of composites, in-the-field repair of polymeric and composite structures, wearable and portable devices, and de-icing/anti-icing of various structures.

## AUTHOR INFORMATION

### Corresponding Author

**Mostafa Yourdkhani** – Department of Mechanical Engineering, Colorado State University, Fort Collins, Colorado 80523, United States; School of Advanced Materials Discovery, Colorado State University, Fort Collins, Colorado 80523, United States; [orcid.org/0000-0002-6354-1678](https://orcid.org/0000-0002-6354-1678); Email: [yourd@colostate.edu](mailto:yourd@colostate.edu)

### Authors

**Iman Naseri** – Department of Mechanical Engineering, Colorado State University, Fort Collins, Colorado 80523, United States

**Morteza Ziaee** – Department of Mechanical Engineering, Colorado State University, Fort Collins, Colorado 80523, United States

**Zach N. Nilsson** – Department of Chemistry, Colorado State University, Fort Collins, Colorado 80523, United States; [orcid.org/0000-0002-2003-2232](https://orcid.org/0000-0002-2003-2232)

**Danielle R. Lustig** – Department of Chemistry, Colorado State University, Fort Collins, Colorado 80523, United States

Complete contact information is available at: <https://pubs.acs.org/10.1021/acsomega.1c06572>

### Author Contributions

The manuscript was written through contributions of all authors. All authors have given approval to the final version of the manuscript.

### Notes

The authors declare no competing financial interest.

## ACKNOWLEDGMENTS

This work was supported by startup funds from the Department of Mechanical Engineering at Colorado State University. The authors would like to thank the staff members of the Nancy Richardson Design Center at Colorado State University for their help and support with using CO<sub>2</sub> laser and Dr. Justin Sambur for providing access to Raman spectrometer. I.N. would like to acknowledge the summer internship award from the Energy Institute at Colorado State University.

## REFERENCES

- (1) Jeong, Y. G.; Jeon, G. W. Microstructure and Performance of Multiwalled Carbon Nanotube/*m*-Aramid Composite Films as Electric Heating Elements. *ACS Appl. Mater. Interfaces* **2013**, *5*, 6527–6534.
- (2) Tarfaoui, M.; El Moumen, A.; Boehle, M.; Shah, O.; Lafdi, K. Self-Heating and Deicing Epoxy/Glass Fiber Based Carbon Nanotubes Buckypaper Composite. *J. Mater. Sci.* **2019**, *54*, 1351–1362.
- (3) Lee, J.; Ni, X.; Daso, F.; Xiao, X.; King, D.; Gómez, J. S.; Varela, T. B.; Kessler, S. S.; Wardle, B. L. Advanced Carbon Fiber Composite Out-of-Autoclave Laminated Manufacture via Nanostructured out-of-Oven Conductive Curing. *Compos. Sci. Technol.* **2018**, *166*, 150–159.
- (4) Wang, T.; Zheng, Y.; Raji, A.-R. O.; Li, Y.; Sikkema, W. K. A.; Tour, J. M. Passive Anti-Icing and Active Deicing Films. *ACS Appl. Mater. Interfaces* **2016**, *8*, 14169–14173.
- (5) Zhan, Y.; Li, Y.; Meng, Y.; Xie, Q.; Lavorgna, M. Electric Heating Behavior of Reduced Oxide Graphene/Carbon Nanotube/Natural Rubber Composites with Macro-Porous Structure and Segregated Filler Network. *Polymers* **2020**, *12*, No. 2411.
- (6) Wu, Z. P.; Wang, J. N. Preparation of Large-Area Double-Walled Carbon Nanotube Films and Application as Film Heater. *Phys. E* **2009**, *42*, 77–81.
- (7) Li, Y.; Zhang, Z.; Li, X.; Zhang, J.; Lou, H.; Shi, X.; Cheng, X.; Peng, H. A Smart, Stretchable Resistive Heater Textile. *J. Mater. Chem. C* **2017**, *5*, 41–46.
- (8) Hong, S.; Lee, H.; Lee, J.; Kwon, J.; Han, S.; Suh, Y. D.; Cho, H.; Shin, J.; Yeo, J.; Ko, S. H. Highly Stretchable and Transparent Metal Nanowire Heater for Wearable Electronics Applications. *Adv. Mater.* **2015**, *27*, 4744–4751.
- (9) Park, J.; Han, D.; Choi, S.; Kim, Y.; Kwak, J. Flexible Transparent Film Heaters Using a Ternary Composite of Silver Nanowire, Conducting Polymer, and Conductive Oxide. *RSC Adv.* **2019**, *9*, 5731–5737.
- (10) Cheng, Y.; Zhang, H.; Wang, R.; Wang, X.; Zhai, H.; Wang, T.; Jin, Q.; Sun, J. Highly Stretchable and Conductive Copper Nanowire Based Fibers with Hierarchical Structure for Wearable Heaters. *ACS Appl. Mater. Interfaces* **2016**, *8*, 32925–32933.
- (11) Lin, S.-Y.; Zhang, T.-Y.; Lu, Q.; Wang, D.-Y.; Yang, Y.; Wu, X.-M.; Ren, T.-L. High-Performance Graphene-Based Flexible Heater for Wearable Applications. *RSC Adv.* **2017**, *7*, 27001–27006.
- (12) Kim, D.; Zhu, L.; Jeong, D.-J.; Chun, K.; Bang, Y.-Y.; Kim, S.-R.; Kim, J.-H.; Oh, S.-K. Transparent Flexible Heater Based on Hybrid of Carbon Nanotubes and Silver Nanowires. *Carbon* **2013**, *63*, 530–536.
- (13) Park, T. H.; Yu, S.; Koo, M.; Kim, H.; Kim, E. H.; Park, J.-E.; Ok, B.; Kim, B.; Noh, S. H.; Park, C.; Kim, E.; Koo, C. M.; Park, C. Shape-Adaptable 2D Titanium Carbide (MXene) Heater. *ACS Nano* **2019**, *13*, 6835–6844.
- (14) Wang, Y.; Zhang, P.; Liu, F.; Luo, S. Laser-Induced Freestanding Graphene Papers: A New Route of Scalable Fabrication with Tunable Morphologies and Properties for Multifunctional Devices and Structures. *Small* **2018**, *14*, No. 1802350.
- (15) Ye, R.; James, D. K.; Tour, J. M. Laser-Induced Graphene: From Discovery to Translation. *Adv. Mater.* **2019**, *31*, No. 1803621.
- (16) Kong, D.; Kang, M.; Kim, K. Y.; Jang, J.; Cho, J.; In, J. B.; Lee, H. Hierarchically Structured Laser-Induced Graphene for Enhanced Boiling on Flexible Substrates. *ACS Appl. Mater. Interfaces* **2020**, *12*, 37784–37792.
- (17) Park, H.; Kim, M.; Kim, B. G.; Kim, Y. H. Electronic Functionality Encoded Laser-Induced Graphene for Paper Electronics. *ACS Appl. Mater. Interfaces* **2020**, *3*, 6899–6904.
- (18) Beckham, J. L.; Li, J. T.; Stanford, M. G.; Chen, W.; McHugh, E. A.; Advincula, P. A.; Wyss, K. M.; Chyan, Y.; Boldman, W. L.; Rack, P. D.; Tour, J. M. High-Resolution Laser-Induced Graphene from Photoresist. *ACS Nano* **2021**, *15*, 8976–8983.
- (19) Chyan, Y.; Ye, R.; Li, Y.; Singh, S. P.; Arnusch, C. J.; Tour, J. M. Laser-Induced Graphene by Multiple Lasing: Toward Electronics on Cloth, Paper, and Food. *ACS Nano* **2018**, *12*, 2176–2183.
- (20) Dallinger, A.; Keller, K.; Fitzek, H.; Greco, F. Stretchable and Skin-Conformable Conductors Based on Polyurethane/Laser-Induced Graphene. *ACS Appl. Mater. Interfaces* **2020**, *12*, 19855–19865.
- (21) Kulyk, B.; Silva, B. F. R.; Carvalho, A. F.; Silvestre, S.; Fernandes, A. J. S.; Martins, R.; Fortunato, E.; Costa, F. M. Laser-Induced Graphene from Paper for Mechanical Sensing. *ACS Appl. Mater. Interfaces* **2021**, *13*, 10210–10221.
- (22) Huang, Y.; Tao, L.-Q.; Yu, J.; Zheng, K.; Wang, G.; Chen, X. Improved Performance of Flexible Graphene Heater Based on Repeated Laser Writing. *IEEE Electron Device Lett.* **2020**, *41*, 501–504.
- (23) Thamaraiselvan, C.; Thakur, A. K.; Gupta, A.; Arnusch, C. J. Electrochemical Removal of Organic and Inorganic Pollutants Using Robust Laser-Induced Graphene Membranes. *ACS Appl. Mater. Interfaces* **2021**, *13*, 1452–1462.
- (24) Xu, Y.; Fei, Q.; Page, M.; Zhao, G.; Ling, Y.; Chen, D.; Yan, Z. Laser-Induced Graphene for Bioelectronics and Soft Actuators. *Nano Res.* **2021**, *14*, 3033–3050.
- (25) Zhang, C.; Peng, Z.; Huang, C.; Zhang, B.; Xing, C.; Chen, H.; Cheng, H.; Wang, J.; Tang, S. High-Energy All-in-One Stretchable Micro-Supercapacitor Arrays Based on 3D Laser-Induced Graphene Foams Decorated with Mesoporous ZnP Nanosheets for Self-Powered Stretchable Systems. *Nano Energy* **2021**, *81*, No. 105609.
- (26) Bobinger, M. R.; Romero, F. J.; Salinas-Castillo, A.; Becherer, M.; Lugli, P.; Morales, D. P.; Rodríguez, N.; Rivadeneyra, A. Flexible and Robust Laser-Induced Graphene Heaters Photothermally Scribed on Bare Polyimide Substrates. *Carbon* **2019**, *144*, 116–126.
- (27) Chen, J.; Wang, Y.; Liu, F.; Luo, S. Laser-Induced Graphene Paper Heaters with Multimodally Patternable Electrothermal Performance for Low-Energy Manufacturing of Composites. *ACS Appl. Mater. Interfaces* **2020**, *12*, 23284–23297.
- (28) Liu, F.; Wang, G.; Ding, X.; Luo, S. Multifunctional Laser-Induced Graphene Enabled Polymeric Composites. *Compos. Commun.* **2021**, *25*, No. 100714.
- (29) Wang, H.; Wang, H.; Wang, Y.; Su, X.; Wang, C.; Zhang, M.; Jian, M.; Xia, K.; Liang, X.; Lu, H.; Li, S.; Zhang, Y. Laser Writing of Janus Graphene/Kevlar Textile for Intelligent Protective Clothing. *ACS Nano* **2020**, *14*, 3219–3226.
- (30) Nasser, J.; Groo, L.; Zhang, L.; Sodano, H. Laser Induced Graphene Fibers for Multifunctional Aramid Fiber Reinforced Composite. *Carbon* **2020**, *158*, 146–156.
- (31) Steinke, K.; Groo, L.; Sodano, H. A. Laser Induced Graphene for In-Situ Ballistic Impact Damage and Delamination Detection in Aramid Fiber Reinforced Composites. *Compos. Sci. Technol.* **2021**, *202*, No. 108551.
- (32) Robertson, I. D.; Yourdkhani, M.; Centellas, P. J.; Aw, J. E.; Ivanoff, D. G.; Goli, E.; Lloyd, E. M.; Dean, L. M.; Sottos, N. R.; Geubelle, P. H.; Moore, J. S.; White, S. R. Rapid Energy-Efficient Manufacturing of Polymers and Composites via Frontal Polymerization. *Nature* **2018**, *557*, 223–227.
- (33) Lamberti, A.; Perrucci, F.; Caprioli, M.; Serrapede, M.; Fontana, M.; Bianco, S.; Ferrero, S.; Tresso, E. New Insights on Laser-Induced Graphene Electrodes for Flexible Supercapacitors: Tunable Morphology and Physical Properties. *Nanotechnology* **2017**, *28*, No. 174002.
- (34) Mahmood, F.; Zhang, C.; Xie, Y.; Stalla, D.; Lin, J.; Wan, C. Transforming Lignin into Porous Graphene via Direct Laser Writing for Solid-State Supercapacitors. *RSC Adv.* **2019**, *9*, 22713–22720.
- (35) d'Amora, M.; Lamberti, A.; Fontana, M.; Giordani, S. Toxicity Assessment of Laser-Induced Graphene by Zebrafish during Development. *J. Phys. Mater.* **2020**, *3*, No. 034008.
- (36) Groo, L.; Nasser, J.; Inman, D.; Sodano, H. Laser Induced Graphene for in Situ Damage Sensing in Aramid Fiber Reinforced Composites. *Compos. Sci. Technol.* **2021**, *201*, No. 108541.
- (37) Gueye, M. N.; Carella, A.; Demadrille, R.; Simonato, J.-P. All-Polymeric Flexible Transparent Heaters. *ACS Appl. Mater. Interfaces* **2017**, *9*, 27250–27256.
- (38) Vivaldi, F. M.; Dallinger, A.; Bonini, A.; Poma, N.; Sembranti, L.; Biagini, D.; Salvo, P.; Greco, F.; Francesco, F. D. Three-

Dimensional (3D) Laser-Induced Graphene: Structure, Properties, and Application to Chemical Sensing. *ACS Appl. Mater. Interfaces* **2021**, *13*, 30245–30260.

(39) Yao, S.; Cui, J.; Cui, Z.; Zhu, Y. Soft Electrothermal Actuators Using Silver Nanowire Heaters. *Nanoscale* **2017**, *9*, 3797–3805.